Spontaneous microcavity-polariton coherence across the parametric threshold: Quantum Monte Carlo studies

Iacopo Carusotto[1,*] and Cristiano Ciuti[2]
[1]*BEC-INFM and Dipartimento di Fisica, Università di Trento, 38050 Povo, Italy*
[2]*Laboratoire Pierre Aigrain, École Normale Supérieure, 24 rue Lhomond, F-75231 Paris Cedex 05, France*
(Received 21 April 2005; revised manuscript received 1 July 2005; published 21 September 2005)

We investigate the appearance of spontaneous coherence in the parametric emission from planar semiconductor microcavities in the strong coupling regime. Calculations are performed by means of a quantum Monte Carlo technique based on the Wigner representation of the coupled exciton and cavity-photon fields. The numerical results are interpreted in terms of a nonequilibrium phase transition occurring at the parametric oscillation threshold: below the threshold, the signal emission is incoherent, and both the first and the second-order coherence functions have a finite correlation length which becomes macroscopic as the threshold is approached. Above the threshold, the emission is instead phase coherent over the whole two-dimensional sample and intensity fluctuations are suppressed. Similar calculations for quasi-one-dimensional microcavities show that in this case the phase coherence of the signal emission has a finite extension even above the threshold, while intensity fluctuations are suppressed.

DOI: 10.1103/PhysRevB.72.125335 PACS number(s): 71.36.+c, 42.50.Ar, 42.65.Yj, 02.70.Uu

I. INTRODUCTION

The recent progresses in the growth and manipulation techniques of semiconductor heterostructures have recently led to the realization of planar semiconductor microcavities in which a cavity-photonic mode is strongly coupled to an excitonic transition, so that the resulting elementary excitations consist of linear superpositions of cavity-photon and exciton, the so-called polaritons.[1–3] The polaritons satisfy the Bose statistics, at least in a low-density regime, and have recently started to be considered as potential candidates for the study of many-body effects, e.g., superfluidity,[4] in regimes completely different from the ones usually considered in experiments with helium fluids[5] or ultracold atomic gases.[6]

A further advantage of polaritonic systems consists of the fact that polaritons can be optically injected in the cavity by simply shining an incident light beam onto it, and their properties can then be inferred from the observation of the emitted light. In particular, the coherence properties of the light emission closely reproduce the ones of the in-cavity polaritonic field.[7]

Thanks to their excitonic component, polaritons have strong binary interactions, which have been exploited to obtain spectacular polariton amplification and optical parametric oscillation effects.[3,8–10] Differently from conventional optical resonators with a discrete set of optical modes, planar microcavities are spatially extended systems with a continuum of transverse modes and the parametric oscillation process automatically selects the most favorable one in which to generate the coherent signal field.

Simultaneously with these experiments, an active debate has taken place in the community about the relation between the appearance of spontaneous coherence in optical parametric oscillation in planar microcavities and Bose-Einstein condensation of excitons.[11] The present paper is devoted to shining a light on analogies and differences between the two phenomena: both of them are in fact characterized by the appearance of coherence and long-range order in a Bose field.[6,12,13] There is, however, a major difference: while Bose-Einstein condensation is an equilibrium phenomenon, parametric oscillation takes place in intrinsically out-of-equilibrium systems, where the stationary state arises from a dynamical equilibrium between the driving by the pump and the dissipative effects due to losses. From this point of view, the parametric oscillation threshold is closely related to the laser threshold,[14,15] although standard laser cavities have a finite number of discrete modes.

In order to perform quantitative calculations, a Monte Carlo technique based on the Wigner representation of a quantum field[16] has been generalized to the case of a pair of coupled excitonic and cavity-photonic fields and the resulting numerical code has been used to calculate the one-time correlation functions of the in-cavity field in the stationary state, in particular the first- and second-order ones. As already mentioned, these univocally determine the spatial coherence properties of the emitted light which can be measured in the experiments.

The advantages of the Wigner–Monte Carlo approach with respect to previous works on the subject[17] are manyfold: first of all, we keep track in a complete way of the fluctuations of the polaritonic field, even in the critical region around the threshold, where fluctuations are large and the linearized approaches around the mean-field[9,18,19] fail. Furthermore, no few-mode approximation[19–22] is here performed: the parametric emission into all available modes is automatically taken into account, as well as the correlations between all modes.

Above threshold, the signal emission in planar microcavity geometries occurs in the single, most favorable, mode (which the numerical code is able to automatically select) and therefore shows the typical spatial coherence properties of a Bose-Einstein condensate. As it is not inherited from the pump beam, this coherence is a *spontaneous* one.

On the other hand, the parametric emission from reduced-dimensionality systems such as photon wires[23] shows dramatically different properties: as long-wavelength fluctuations of the signal phase are here able to destroy the long-range spatial coherence, the threshold is no longer well defined and is replaced by a smooth crossover where a local order sets in and the intensity fluctuations of the signal emission are suppressed. Such a behavior is closely related to the so-called quasicondensation phenomenon of equilibrium Bose gases in reduced dimensionalities.[24–26] Related questions about the spontaneous appearance of long-range coherence and the effect of a reduced dimensionality have been recently adressed[27,28] for the simpler case of a parametric oscillator formed by a planar resonator containing a slab of generic $\chi^{(2)}$ medium without any excitonic resonance.

The plan of the present paper is the following. In Sec. II we introduce the field-theoretical Hamiltonian of the system and we relate the properties of the emitted light to the ones of the in-cavity polaritonic field. In Sec. III, we work out the corresponding mean-field theory and we use it to identify the parameter range which is most suited for the following analysis. In Sec. IV, we review the Wigner representation formalism and we generalize it to the case of coupled cavity-photon and exciton fields. We also describe the principles of the numerical code used to obtain the results which are discussed in the following. In Sec. V, the central numerical results of the paper are shown: the behavior of the first- and second-order coherence properties of the signal emission are presented for pump parameters spanning across the parametric threshold. These results are the basis of the discussion of the following Sec. VI, where analogies and differences between our driven-dissipative system and the Bose-Einstein condensation phenomenon of equilibrium statistical mechanics are pointed out. In Sec. VII, an alternative interpretation of the parametric threshold in terms of modulation instability and spontaneous breaking of the translational symmetry is given and its consequences on the intensity correlation function are put forward. The effect of a reduced dimensionality is discussed in Sec. VIII, where the link with the concept of quasi-condensate is evidentiated. Finally, in Sec. IX we give our conclusions, and we sketch the perspectives of the work.

II. THE SYSTEM HAMILTONIAN

A model which is commonly used to describe a planar microcavity with a quantum well excitonic resonance strongly coupled to the cavity mode is based on the field-theoretical Hamiltonian[17]

$$\begin{aligned}\mathcal{H} = &\int d\mathbf{x} \sum_{ij=\{X,C\}} \hat{\Psi}_i^\dagger(\mathbf{x})[\mathbf{h}_{ij}^0 + V_i(\mathbf{x})\delta_{ij}]\hat{\Psi}_j(\mathbf{x}) \\ &+ \frac{\hbar g}{2}\int d\mathbf{x}\hat{\Psi}_X^\dagger(\mathbf{x})\hat{\Psi}_X^\dagger(\mathbf{x})\hat{\Psi}_X(\mathbf{x})\hat{\Psi}_X(\mathbf{x}) \\ &+ \int d\mathbf{x}\,\hbar\beta_{\mathrm{inc}}E_p(\mathbf{x},t)\hat{\Psi}_C^\dagger(\mathbf{x}) + \mathrm{H.c.}, \end{aligned} \tag{1}$$

where $\mathbf{x}$ is the in-plane spatial position. The field operators $\Psi_{X,C}(\mathbf{x})$, respectively, describe excitons (X) and cavity photons (C) and, provided the exciton density is much lower than the saturation density n_{sat},[17] they satisfy Bose commutation rules $[\hat{\Psi}_i(\mathbf{x}),\hat{\Psi}_j^\dagger(\mathbf{x}')]=\delta^2(\mathbf{x}-\mathbf{x}')\delta_{ij}$. For the sake of simplicity, we consider here a single polarization state, but a generalization of Eq. (1) to include several polarization states and describe the spin dynamics discussed, e.g., in Ref. 29 is straightforward.

In the $\mathbf{k}$-space representation, the single-particle Hamiltonian $\mathbf{h}^0$ has the simple form

$$\mathbf{h}^0(\mathbf{k}) = \hbar\begin{pmatrix}\omega_X(\mathbf{k}) & \Omega_R \\ \Omega_R & \omega_C(\mathbf{k})\end{pmatrix}, \tag{2}$$

where $\omega_C(\mathbf{k})=\omega_C^0\sqrt{1+\mathbf{k}^2/k_z^2}$ is the cavity dispersion as a function of the in-plane wave vector $\mathbf{k}$ and k_z is the quantized photon wave vector in the growth direction. The exciton dispersion is instead much weaker and can be well approximated by a constant $\omega_X(\mathbf{k})=\omega_X$. The quantity Ω_R is the Rabi frequency of the exciton-cavity photon coupling. From Eq. (2), one obtains the real-space form which appears in Eq. (1) by simply replacing the wave vector $\mathbf{k}$ with the spatial gradient $-i\nabla$.

The eigenmodes of the linear Hamiltonian (2) are linear combinations the cavity photonic and excitonic modes. They are called upper (UP) and lower (LP) polariton, and are defined by the eigenvalue equation

$$\mathbf{h}^0(\mathbf{k})\begin{pmatrix}X_{\mathrm{LP(UP)}}(\mathbf{k}) \\ C_{\mathrm{LP(UP)}}(\mathbf{k})\end{pmatrix} = \hbar\omega_{\mathrm{LP(UP)}}(\mathbf{k})\begin{pmatrix}X_{\mathrm{LP(UP)}}(\mathbf{k}) \\ C_{\mathrm{LP(UP)}}(\mathbf{k})\end{pmatrix}, \tag{3}$$

where $\omega_{\mathrm{LP(UP)}}(\mathbf{k})$ are the frequency dispersions of respectively the lower (LP) and the upper (UP) polaritons, and the coefficients $X_{\mathrm{LP(UP)}}(\mathbf{k})$ and $C_{\mathrm{LP(UP)}}(\mathbf{k})$ are the so-called Hopfield coefficients. $V_{X,C}(\mathbf{x})$ are external potential terms acting on the excitonic and photonic fields and can be used to model etched cavities.[23]

Exciton-exciton interactions are modeled by a local interaction term, quartic in the exciton field operator, with a positive interaction constant $g>0$. The strength g of these repulsive interactions depends on the details of the microcavity system, in particular of the quantum well exciton. In the absence of a complete theoretical analysis,[30,45] g can be fitted from experimental data. Remarkably, the experimental value is not far from the prediction of theoretical calculations within the Born approximation[31]

$$g = \frac{6e^2\lambda_X}{\epsilon} \tag{4}$$

that will be used in the following; here, λ_X is the two-dimensional exciton radius and ϵ is the static dielectric constant of the quantum well. As the excitonic transition has a finite saturation density, an additional term describing the anharmonic exciton-photon coupling may play an important role in some regimes. In the one considered in the present study, it has a negligible effect.[17]

Differently from other Bose systems such as ultracold trapped atoms or liquid helium, our polaritonic system is intrinsically out of equilibrium. Polaritons are in fact injected in the cavity by incident light beams and decay through sev-

eral dissipative channels. In the present paper, polaritons are coherently injected in the cavity by a coherent *pump* laser, which is taken into account in the Hamiltonian (1) by the driving term proportional to the incident electric field $E_p(\mathbf{x},t)$ of the pump. For a given cavity, the coefficient β_{inc} can be calculated from the reflectivity of the front mirror through which the cavity is excited.[16] Both the spatial and the temporal dependences of $E_p(\mathbf{x},t)$ can be experimentally controlled, so to obtain a variety of different temporal (e.g., monochromatic, bichromatic, pulsed, etc.) and spatial (e.g., plane wave, Gaussian, optical vortex, etc.) patterns.[32]

Dissipative effects lead to a damping of both the excitonic and cavity photonic fields. Using the standard quantum theory of damping, they can be modelled by additional terms in the master equation giving the time evolution of the density matrix ρ of the system[16]

$$\frac{d\rho}{dt} = -\frac{i}{\hbar}[\mathcal{H},\rho] + \int \frac{d\mathbf{k}}{(2\pi)^2} \sum_{i=\{X,C\}} \gamma_i(\mathbf{k}) \left[\hat{\Psi}_i(\mathbf{k}) \rho \hat{\Psi}_i^\dagger(\mathbf{k}) - \frac{1}{2}[\hat{\Psi}_i^\dagger(\mathbf{k})\hat{\Psi}_i(\mathbf{k})\rho + \rho\hat{\Psi}_i^\dagger(\mathbf{k})\hat{\Psi}_i(\mathbf{k})] \right]. \quad (5)$$

The operators $\hat{\Psi}_{X,C}(\mathbf{k})$ are the Fourier transform of the field operators $\hat{\Psi}_{X,C}(\mathbf{x})$. In the present paper, we shall consider the case of momentum-independent $\gamma_{C,X}$ which summarize dissipative effects of different origin, e.g., excitonic scattering and nonradiative recombination, background absorption by the material forming the structure as well as radiative emission into the continuum of modes outside the cavity.

From the experimental point of view, information on the state of the polariton field in the cavity is generally retrieved by detecting and characterizing the light emission from the cavity through either the front or the back mirror. This procedure has recently been used to determine the first- and second-order correlation functions of the polaritonic field by measuring the coherence and noise properties of the emitted light.[7]

In particular, the expectation values of the normally-ordered operators for the light emitted through the back mirror (called in the following "transmitted" light)[46] are related to the cosrresponding expectation values for the photonic component of the in-cavity polaritonic field. Assuming the transmittivity of the back mirror to be independent of the incidence angle (i.e., the in-plane wave vector $\mathbf{k}$) and of the frequency, this relation is a simple proportionality one, with a proportionality coefficient $\beta_{\rm tr}$ which can be calculated starting from the back mirror transmittivity.[16]

The first-order coherence matrix of the electric field in the near-field region is then

$$\langle \hat{E}_{\rm tr}^\dagger(\mathbf{x})\hat{E}_{\rm tr}(\mathbf{x}')\rangle = |\beta_{\rm tr}|^2 \langle \hat{\Psi}_C^\dagger(\mathbf{x})\hat{\Psi}_C(\mathbf{x}')\rangle, \quad (6)$$

where the operator $\hat{E}_{\rm tr}(\mathbf{x})$ describes the electric field radiated outside the cavity but measured still very close to the back mirror. Similar formulas hold for the far-field properties of the emission, e.g., its angular pattern:

$$\langle \hat{E}_{\rm tr}^\dagger(\mathbf{k})\hat{E}_{\rm tr}(\mathbf{k})\rangle = |\beta_{\rm tr}|^2 n_C(\mathbf{k}) = |\beta_{\rm tr}|^2 \langle \hat{\Psi}_C^\dagger(\mathbf{k})\hat{\Psi}_C(\mathbf{k})\rangle \quad (7)$$

as well as for the higher-order, normally ordered moments such as

$$\langle \hat{E}_{\rm tr}^\dagger(\mathbf{k})\hat{E}_{\rm tr}^\dagger(\mathbf{k}')\hat{E}_{\rm tr}(\mathbf{k}')\hat{E}_{\rm tr}(\mathbf{k})\rangle = |\beta_{\rm tr}|^4 \langle \hat{\Psi}_C^\dagger(\mathbf{k})\hat{\Psi}_C^\dagger(\mathbf{k}')\hat{\Psi}_C(\mathbf{k}')\hat{\Psi}_C(\mathbf{k})\rangle. \quad (8)$$

If the system is driven close to resonance with the lower polariton frequency, and the interaction energy is much smaller than the exciton-cavity photon Rabi frequency Ω_R, the polariton field is mostly composed of polaritons of the lower (LP) branch. In this case, the photonic and excitonic component of the polaritonic field have a simple expression[17] in terms of the lower polariton (bosonic) operators $\hat{\Psi}_{\rm LP}$:

$$\hat{\Psi}_{\rm LP}(\mathbf{k}) = X_{\rm LP}(\mathbf{k})\hat{\Psi}_X(\mathbf{k}) + C_{\rm LP}(\mathbf{k})\hat{\Psi}_C(\mathbf{k}) \quad (9)$$

and of the Hopfield coefficients introduced in Eq. (3). For instance, the angular emission pattern (7) is simply related to the occupation number of the lower polariton by

$$\langle \hat{E}_{\rm tr}^\dagger(\mathbf{k})\hat{E}_{\rm tr}(\mathbf{k})\rangle \simeq |\beta_{\rm tr}|^2 |C_{\rm LP}(\mathbf{k})|^2 \langle \hat{\Psi}_{\rm LP}^\dagger(\mathbf{k})\hat{\Psi}_{\rm LP}(\mathbf{k})\rangle. \quad (10)$$

As the photonic component $C_{\rm LP}$ of the lower polariton is a decreasing function of the wave vector k, the radiative emission strength is largest for the low-$\mathbf{k}$ polaritons.

III. MEAN-FIELD THEORY

A simple way of coping with the field Hamiltonian (1) is to study the corresponding classical field theory once the quantum field operators $\Psi_{X,C}(\mathbf{x})$ are replaced with classical $\mathbf{C}$ number fields $\psi_{X,C}(\mathbf{x})$ defined as the expectation value of the quantum field $\psi_{X,C}(\mathbf{x}) = \langle \Psi_{X,C}(\mathbf{x})\rangle$. For a system of weakly interacting bosons such as microcavity polaritons, fluctuations are generally weak provided the mean-field solution is dynamically stable, so that the mean-field solution provides accurate predictions for the coherent part of the polariton field, and therefore the coherent emission from the microcavity. This includes, e.g., resonant Rayleigh scattering in the presence of defects.[4] In the present paper, the mean-field prediction for the threshold intensity will be used as a guideline in the choice of parameters to be used in the numerical calculations.

As we are most interested in the basic properties of the parametric instability threshold, we have tried to identify a configuration where the intrinsic phenomenology is not masked by additional effects. In particular, we have considered the case of a homogeneous cavity with no external potential $V_{X,C}=0$ and a transversally homogeneous, monochromatic and cw laser field of frequency ω_p which incides on the cavity at an angle θ_p with the normal to the cavity plane. Provided the beam actually used in the experiment is wide enough in the transverse direction, this approximation is expected to be accurate. The pump electric field has then the simple form

$$E_p(\mathbf{x},t) = E_p e^{i(\mathbf{k}_p\cdot\mathbf{x}-\omega_p t)}, \tag{11}$$

the wave vector $\mathbf{k}_p$ being fixed by the incidence angle through $k_p = \sin\theta_p \omega_p/c$. The incident intensity I_p is proportional to $|E_p|^2$:

$$I_p = \frac{c}{2\pi}|E_p|^2. \tag{12}$$

Given the translational symmetry of the system, we can look for stationary solutions in the same plane-wave form $\psi_{X,C}(\mathbf{x},t) = \psi^{ss}_{X,C} e^{i(\mathbf{k}_p\mathbf{x}-\omega_p t)}$ as the incident field. The coefficients $\psi^{ss}_{X,C}$ can be obtained from the equation of state

$$\left(\omega_X(\mathbf{k}_p) - \omega_p - \frac{i}{2}\gamma_X + g|\psi^{ss}_X|^2\right)\psi^{ss}_X + \Omega_R\psi^{ss}_C = 0, \tag{13}$$

$$\left(\omega_C(\mathbf{k}_p) - \omega_p - \frac{i}{2}\gamma_C\right)\psi^{ss}_C + \Omega_R\psi^{ss}_X = -\beta_{\mathrm{inc}}E_p \tag{14}$$

and the stability of the solution has to be verified by looking at the eigenvalues of the Bogoliubov matrix[4]

$$\mathcal{L} = \begin{pmatrix} \omega_X + 2g|\psi^{ss}_X|^2 - \omega_p - \frac{i\gamma_X}{2} & \Omega_R & g\psi^{ss2}_X e^{2i\mathbf{k}_p\mathbf{x}} & 0 \\ \Omega_R & \omega_C(-i\nabla) - \omega_p - \frac{i\gamma_C}{2} & 0 & 0 \\ -g\psi^{ss*2}_X e^{-2i\mathbf{k}_p\mathbf{x}} & 0 & -(\omega_X + 2g|\psi^{ss}_X|^2) + \omega_p - \frac{i\gamma_X}{2} & -\Omega_R \\ 0 & 0 & -\Omega_R & -\omega_C(-i\nabla) + \omega_p - \frac{i\gamma_C}{2} \end{pmatrix}. \tag{15}$$

If the imaginary parts of all the eigenvalues $\omega^{\pm}_{\mathrm{UP,LP}}(\mathbf{k})$ of the Bogoliubov matrix $\mathcal{L}$ are negative for all $\mathbf{k}$, the mean-field solution is dynamically stable; if at least one of them is positive, a different, spatially structured, stationary solution has to be found, e.g., with a sinusoidal intensity profile, and its stability has again to be verified by means of the appropriate Bogoliubov matrix. An analytical study of the mean-field stationary state in the parametric oscillation regime when translational symmetry is broken is beyond the scope of the present work. Simple discussions under a simple three-mode approximation taking into account only the pump, the signal and the idler modes can be found, e.g., in Refs. 19–22.

In order to keep the physics the simplest, we have chosen a fixed value of the pump intensity I_p and we have spanned its frequency ω_p from far below the lower polariton frequency at linear regime $\omega_{\mathrm{LP}}(\mathbf{k}_p)$ in the upward direction. The incidence angle θ_p has been taken slightly larger than the so-called magic angle, so that $2\omega_{\mathrm{LP}}(\mathbf{k}_p) > \omega_L(0) + \omega_{\mathrm{LP}}(2\mathbf{k}_p)$. The corresponding Bogoliubov dispersions are plotted in Fig. 1: as expected, the first feature that takes place is the parametric instability when the ± branches, which are coupled by the anti-Hermitian terms of Eq. (15), touch around $\mathbf{k}\approx 0$. This condition $2\omega_p = \omega^+_{\mathrm{LP}}(0) + \omega^+_{\mathrm{LP}}(2\mathbf{k}_p)$ can be interpreted as the parametric process $(\mathbf{k}_p,\mathbf{k}_p)\rightarrow(0,2\mathbf{k}_p)$ becoming resonant on the final state.

For our specific choice of θ_p and ω_p, notice that this happens at a value $\omega_p = \omega^{(c)}_p$ still red detuned with respect to $\omega_{\mathrm{LP}}(\mathbf{k}_p)$. This guarantees that we are still in an optical limiter regime and no single-mode optical bistability effects[4] has yet taken place. In the following of the paper, the frequency $\omega^{(c)}_p$ will be designed as the parametric instability threshold and the wording below/above threshold will refer to ω_p, respectively, red or blue detuned with respect to $\omega^{(c)}_p$. This definition of the threshold in terms of frequency is alternative but equivalent to the standard one in terms of the intensity and allows us to avoid those complicated additional effects that

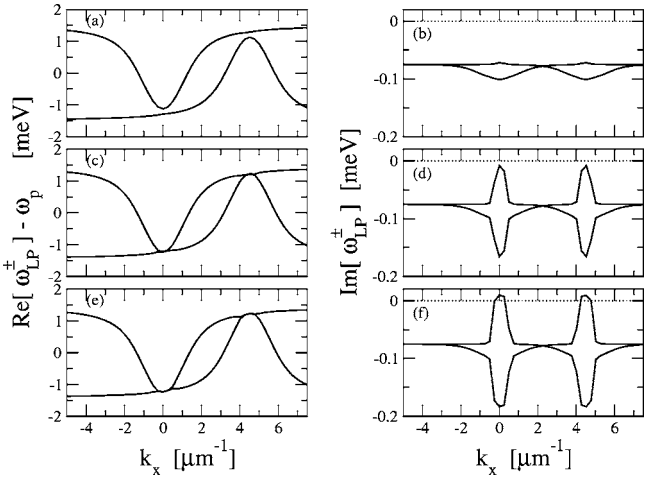

FIG. 1. Real (left) and imaginary (right) parts of the Bogoliubov dispersion for different values of the pump frequency $\hbar\delta_p = \hbar[\omega_p - \omega_{LP}(\mathbf{k}_p)] = -0.65$ meV (a), (b), −0.54 meV (c), (d), −0.49 meV (e), (f). At the mean-field threshold $\hbar\delta_p = \hbar\delta^{(c)}_p \approx -0.52$ meV, the mean-field energy $\hbar g|\psi_X|^2 \simeq 0.13$ meV. For the sake of clarity, only the branches corresponding to the LP have been traced, the UP ones being far away in energy. Cavity parameters: $\hbar\omega^0_C = \hbar\omega_X = 1.4$ eV, $2\hbar\Omega_R = 5$ meV, $\hbar\gamma_X = 0.15$ meV, $\hbar\gamma_C = 0.24$ meV. The lower polariton energy at linear regime is $\hbar\omega_{LP}(\mathbf{k}_p) = 1.39935$ eV.

have been pointed out in Ref. 22. For notational simplicity, we shall also introduce the quantity $\delta_p=\omega_p-\omega_{\mathrm{LP}}(\mathbf{k}_p)$; at the threshold $\delta_p=\delta_p^{(c)}<0$.

IV. THE WIGNER MONTE CARLO METHOD

A more complete analysis of the parametric threshold can be carried out by numerically solving the stochastic equations of the Wigner representation of the quantum Bose field. This technique allows one to study the dynamics of the field taking fully into account the multimode structure of the field and eventually the spontaneous breaking of the translational symmetry, as well as the fluctuations around the mean-field solution, however large they happen to be. In the present section, we shall review the formalism of the Wigner representation of the quantum Bose field as applied to a pair of coupled photonic and excitonic fields with a quartic interaction term. Recently, a similar Wigner approach has been applied to study the dynamical properties of ultracold atomic gases.[33]

The Wigner representation of the two-component quantum Bose field $\hat{\Psi}_i(\mathbf{x})$ $(i=\{X,C\})$ consists of a quasiprobability distribution function $W[\psi_i(\mathbf{x})]$ in the functional space of the **C**-number fields $\psi_i(\mathbf{x})$.[16] Any numerical implementation requires one to work on a discrete and finite spatial grid: in our simulations, a rectangular grid of $\mathcal{N}_x\times\mathcal{N}_y$ points with uniform grid spacings $\ell_{x,y}$ along, respectively, the x, y directions has been used, with periodic boundary conditions. The integration box has therefore sides $L_{x,y}=\mathcal{N}_{x,y}\ell_{x,y}$.

Under a diluteness condition that can be written as $\gamma_i \gg g/dV$ ($dV=\ell_x\ell_y$ being the cell volume), the evolution of the quasiprobability distribution W can be approximated in the so-called "truncated Wigner approximation"[33] by a true Fokker-Planck equation with a positive-definite diffusion matrix and without higher-order derivative terms, which guarantees the positivity of W at all times and the possibility of mapping the problem onto stochastic differential equations for the fields $\psi_i(\mathbf{x})$:

$$d\begin{pmatrix}\psi_X(\mathbf{x})\\ \psi_C(\mathbf{x})\end{pmatrix}=-\frac{i}{\hbar}\left\{\begin{pmatrix}0\\ \hbar\beta_{\mathrm{inc}}E_p(\mathbf{x},t)\end{pmatrix}+\left[\mathbf{h}^0+\begin{pmatrix}V_X(\mathbf{x})+\hbar g\left(|\psi_X(\mathbf{x})|^2-\frac{1}{dV}\right)-\frac{i\gamma_X}{2} & 0\\ 0 & V_C(\mathbf{x})-\frac{i\gamma_C}{2}\end{pmatrix}\right]\begin{pmatrix}\psi_X(\mathbf{x})\\ \psi_C(\mathbf{x})\end{pmatrix}\right\}dt+\frac{1}{\sqrt{4\Delta V}}\begin{pmatrix}\sqrt{\gamma_X}dW_X(\mathbf{x})\\ \sqrt{\gamma_C}dW_C(\mathbf{x})\end{pmatrix}, \tag{16}$$

where $dW_{X,C}(\mathbf{x})$, are zero-mean, independent, complex-valued, white noise terms such that

$$\overline{dW_i(\mathbf{x})dW_j(\mathbf{x}')}=0, \tag{17}$$

$$\overline{dW_i(\mathbf{x})dW_j^*(\mathbf{x}')}=2\ dt\ \delta_{\mathbf{x},\mathbf{x}'}\delta_{ij}. \tag{18}$$

In the most relevant case of an initially empty microcavity, the initial fields at $t=0$ are independent zero-mean complex Gaussian variables such that

$$\overline{\psi_i(\mathbf{x})\psi_j(\mathbf{x})}=0, \tag{19}$$

$$\overline{\psi_i(\mathbf{x})\psi_j^*(\mathbf{x})}=\frac{1}{2\Delta V}\delta_{ij}. \tag{20}$$

In a practical Wigner–Monte Carlo simulation, the Wigner distribution of the initial state at $t=0$ is sampled with a large number $\mathcal{N}$ of independent realizations (the data shown in the present paper have been calculated from a number $\mathcal{N}$ of realizations of the order of a few thousands). They are then let evolve according to the stochastic equation (16) with a random noise which is obviously different for each realization.

The expectation value of any observables at time t is obtained as an average over the different realizations of the corresponding classical quantity, paying attention to the fact that the moments of the Wigner function give the expectation value of totally symmetrized operators, e.g.,

$$\langle O_1\cdots O_N\rangle_W=\frac{1}{N!}\sum_P\langle\hat{O}_{P(1)}\cdots\hat{O}_{P(N)}\rangle, \tag{21}$$

where the sum is taken over all the permutations P of N objects, each of the O_α's stands for some field component $\psi_i(\mathbf{x})$ or $\psi_i^*(\mathbf{x})$ and $\hat{O}_\alpha$ is the corresponding field operator. As a simplest example,

$$\langle\psi_C^*(\mathbf{x})\psi_C(\mathbf{x}')\rangle_W=\frac{1}{2}\langle\hat{\Psi}_C^\dagger(\mathbf{x})\hat{\Psi}_C(\mathbf{x}')+\hat{\Psi}_C(\mathbf{x}')\hat{\Psi}_C^\dagger(\mathbf{x})\rangle. \tag{22}$$

In the following of the paper, we shall use this Wigner–Monte Carlo method to numerically study the one-time correlation functions of the in-cavity fields in the stationary state. These are obtained by letting the evolution to run for a time interval longer than all the characteristic time scales of the problem, until the stationary state is attained (in practice an evolution time of at most 5 ns is used). At this point, the

expectation values of the observables are evaluated from the corresponding averages over the Wigner distribution. Note that we have chosen the excitation parameters in such a way that the pump has a simple optical limiter behavior and complex bistability effects are avoided.

For instance, the first-order correlation function in the near-field has the form

$$\langle \hat{\Psi}_C^\dagger(\mathbf{x})\hat{\Psi}_C(\mathbf{x}')\rangle = \left[\langle \psi_C^*(\mathbf{x})\psi_C(\mathbf{x}')\rangle_W - \frac{\delta_{\mathbf{x},\mathbf{x}'}}{2\Delta V}\right] \tag{23}$$

while the second-order one reads

$$\begin{aligned}\langle \hat{\Psi}_C^\dagger(\mathbf{x})\hat{\Psi}_C^\dagger(\mathbf{x}')\hat{\Psi}_C(\mathbf{x}')\hat{\Psi}_C(\mathbf{x})\rangle &= \left\langle |\psi_C(\mathbf{x})|^2|\psi_C(\mathbf{x}')|^2 - \frac{1}{2\Delta V}(1+\delta_{\mathbf{x},\mathbf{x}'})\right. \\ &\left.\times\left(|\psi_C(\mathbf{x})|^2 + |\psi_C(\mathbf{x}')|^2 - \frac{1}{2\Delta V}\right)\right\rangle_W . \end{aligned} \tag{24}$$

Similar formulas hold for the **k**-space observables which describe the emission pattern in the far field.

The study of multitime correlation functions which are involved in the temporal coherence properties requires the calculation of nontrivial different-time commutators or a specific treatment of quantum noise incident on the cavity.[28] All these issues go beyond the scope of the present work and will be the subject of a forthcoming publication.

V. COHERENCE PROPERTIES OF THE PARAMETRIC EMISSION

The Wigner–Monte Carlo method reviewed in the previous section can be applied to study the parametric emission for ω_p spanning across the threshold. Depending on whether $\omega_p < \omega_p^{(c)}$ or $\omega_p > \omega_p^{(c)}$, the emission shows in fact dramatically different features which appear clearly in the angular intensity pattern of the far-field emission as well as in its first- and second-order coherence properties.

A. Below the parametric instability threshold

1. Far-field angular pattern

Below the threshold, the far-field emission patterns shown in Fig. 2 are characterized by a strong and narrow peak corresponding to the mode at $\mathbf{k}_p$ being directly pumped by the incident laser field, and weaker and broader peaks corresponding to the luminescence from other modes due to parametric processes $(\mathbf{k}_p,\mathbf{k}_p)\rightarrow(\mathbf{k}_s,\mathbf{k}_i=2\mathbf{k}_p-\mathbf{k}_s)$. As the pump frequency ω_p is increased and approaches the threshold at $\omega_p^{(c)}$, not only does the intensity of the luminescence peaks increase, but it is also spectrally narrowed in **k** space, until it becomes a very narrow peak in the vicinity of the instability threshold.

As discussed in Ref. 34 and experimentally verified in Ref. 35, the parametric luminescence has remarkable correlations properties, in particular a significant degree of multimode squeezing between the signal and idler. However, as these properties do not play a central role in the coherence properties of the signal alone, we shall not analyze them in detail in the present paper.

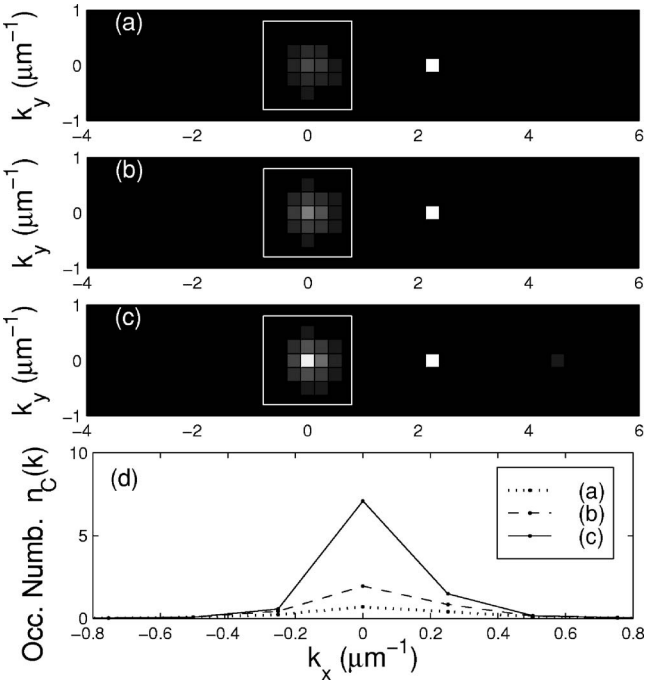

FIG. 2. Far-field emission pattern for increasing values of the pump frequency $\hbar\delta_p=-0.55$ meV (a), -0.53 meV (b) below the mean-field threshold, and -0.52 meV (c) close to the mean-field threshold. The pump mode at $\mathbf{k}_p$ by far saturates the grey scale, while the idler emission is hardly visible on this scale. The solid rectangles indicate the **k**-space region which forms the signal emission. Throughout the whole paper, the correlation functions of the selected signal emission are denoted with a bar (e.g., $\bar{G}^{(2)}$ and $\bar{g}^{(1,2)}$). (d) Cut for $k_y=0$ of the far-field emission pattern shown in panels (a)–(c). For clarity reasons, only the part of the spectrum corresponding to the signal emission is shown. Same cavity and pump parameters as in Fig. 1, physical size of the system $L_x=L_y=25$ μm.

2. First- and second-order coherence

The real space counterpart of the linewidth reduction is an increase of the coherence length. In the experiments,[7] a region S in **k** space around the peak of the signal emission (the region inside the squares in Fig. 2) is selected by means of suitable combination of diaphragms. The corresponding real-space correlation functions are then defined as

$$\bar{G}^{(1)}(\mathbf{x},\mathbf{y}) = \langle \hat{\bar{\Psi}}_C^\dagger(\mathbf{x})\hat{\bar{\Psi}}_C(\mathbf{y})\rangle, \tag{25}$$

$$\bar{G}^{(2)}(\mathbf{x},\mathbf{y}) = \langle \hat{\bar{\Psi}}_C^\dagger(\mathbf{x})\hat{\bar{\Psi}}_C^\dagger(\mathbf{y})\hat{\bar{\Psi}}_C(\mathbf{y})\hat{\bar{\Psi}}_C(\mathbf{x})\rangle \tag{26}$$

in terms of the signal field operators $\hat{\bar{\Psi}}_C(\mathbf{x})$ defined as

$$\hat{\bar{\Psi}}_C(\mathbf{x}) = \sum_{\mathbf{k}\in S}\frac{1}{\sqrt{V}}\hat{\bar{\Psi}}_C(\mathbf{k})e^{i\mathbf{k}\cdot\mathbf{x}}, \tag{27}$$

where the sum over **k** vectors is here restricted to the selected region S only. The bar over $\bar{G}^{(1,2)}$ indicates that these

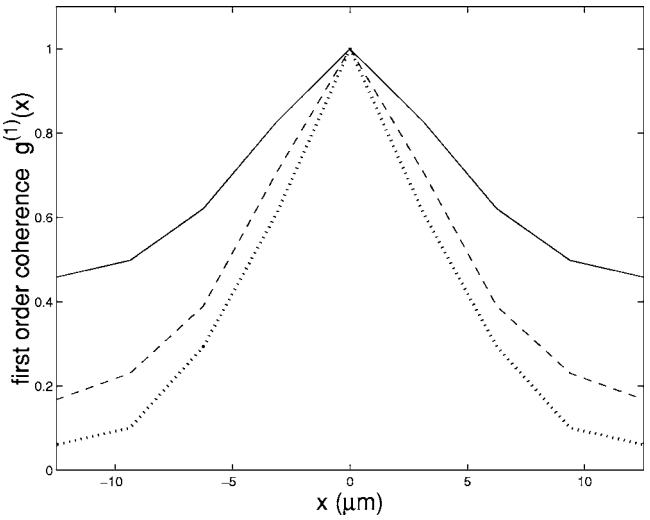

FIG. 3. First-order coherence function $\bar{g}^{(1)}(\mathbf{x})$ of the selected (see solid rectangle in Fig. 2) signal emission for values of the pump frequency $\hbar\delta_p=-0.55$ meV (dotted), $\hbar\delta_p=-0.53$ meV (dashed), and $\hbar\delta_p=-0.52$ meV (solid), respectively, below and around the mean-field threshold. The cavity and the other pump parameters are the same as in Fig. 1.

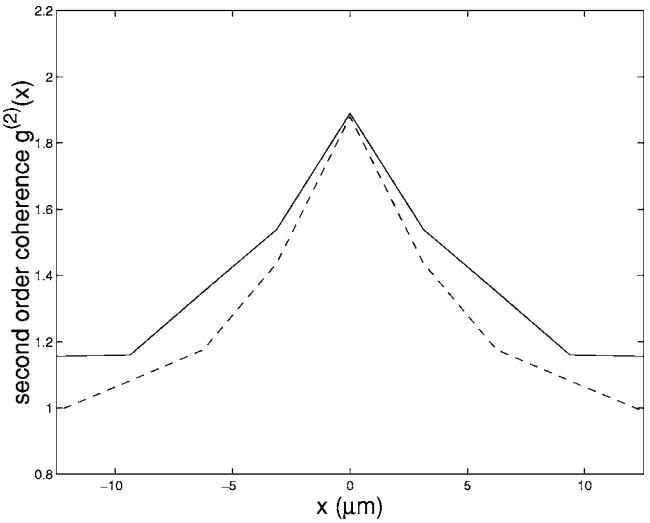

FIG. 4. Second-order coherence function $\bar{g}^{(2)}(\mathbf{x})$ of the selected (see solid rectangle in Fig. 2) signal emission for values of the pump frequency $\hbar\delta_p=-0.53$ meV (dashed) and -0.52 meV (solid), respectively, below and around the mean-field threshold. The cavity and the other pump parameters are the same as in Fig. 1.

correlation functions are restricted to the selected signal emission only. As usual, the translational invariance of the system guarantees that all two point correlation functions depend only on the distance $\mathbf{x}-\mathbf{y}$. In Fig. 3 we have plotted the first order coherence function for the signal emission

$$\bar{g}^{(1)}(\mathbf{x}) = \frac{\bar{G}^{(1)}(\mathbf{y},\mathbf{y}+\mathbf{x})}{\bar{G}^{(1)}(\mathbf{y},\mathbf{y})}. \tag{28}$$

For ω_p well below the threshold, $\bar{g}^{(1)}(\mathbf{x})$ goes from 1 to 0 within a coherence length ℓ_c which according to the Wiener-Khintchine theorem is proportional to the inverse of the $\mathbf{k}$-space linewidth. As the threshold is approached, ℓ_c increases. At the threshold, $\bar{g}^{(1)}(\mathbf{x})$ is everywhere finite so that the coherence extends over the whole (finite) sample. From an experimental point of view, $\bar{g}^{(1)}(\mathbf{x})$ can be measured by first angularly filtering out the emission in the $\mathbf{k}$-space region S centered around $\mathbf{k}_s$, and then performing a sort of Young's two-slit experiment like the one in Ref. 7. The second-order coherence function of the signal emission $\bar{g}^{(2)}$ is defined as

$$\bar{g}^{(2)}(\mathbf{x}) = \frac{\bar{G}^{(2)}(\mathbf{y},\mathbf{y}+\mathbf{x})}{[\bar{G}^{(1)}(\mathbf{y},\mathbf{y})]^2} \tag{29}$$

and experimentally can be accessed by noise correlation experiments like the ones reported in Ref. 7. As previously, the bar over $\bar{g}^{(2)}$ indicates that this coherence function includes the selected signal emission only. For ω_p well below the threshold $\omega_p^{(c)}$, $\bar{g}^{(2)}(\mathbf{x})$ shows the typical Hanbury-Brown and Twiss bunching[36] at short distances $|\mathbf{x}| \ll \ell_c$, where its value is close to 2, and then it tends to 1 for $|\mathbf{x}| \gg \ell_c$. This behavior can be easily understood in terms of the Gaussian structure of the field: well below the threshold, all modes of the coupled excitonic and photonic fields in the microcavity are in a Gaussian state, exception made for the one at $\mathbf{k}_p$ directly driven by the pump. This means that Wick theorem applies and higher-order correlation functions can be consequently factorized into products of first-order ones.[24] As the parametric emission gives nonvanishing anomalous correlations only between the signal and the idler modes, all the anomalous correlations appearing in the Wick factorization of the signal second-order correlation function $\bar{G}^{(2)}(\mathbf{x},\mathbf{y})$ vanish and this can be factorized as

$$\bar{G}^{(2)}(\mathbf{x},\mathbf{y}) \simeq \bar{G}^{(1)}(\mathbf{x},\mathbf{x})\bar{G}^{(1)}(\mathbf{y},\mathbf{y}) + |\bar{G}^{(1)}(\mathbf{x},\mathbf{y})|^2 \tag{30}$$

so that $\bar{g}^{(2)}(\mathbf{x})$ is

$$\bar{g}^{(2)}(\mathbf{x}) \simeq 1 + |\bar{g}^{(1)}(\mathbf{x})|^2. \tag{31}$$

This form is consistent with the numerical results shown in Figs. 3 and 4. In particular, the coherence length of $\bar{G}^{(2)}$ is roughly half the one of $\bar{G}^{(1)}$. Note that the decomposition (30) would not be valid for quantities without a bar, e.g., $G^{(2)}(\mathbf{x})$ that will be introduced in Eq. (33) since in that case the anomalous correlation between signal and idler gives an important contribution. Closer to the threshold, the field is no longer in a Gaussian state: the short-distance value $\bar{g}^{(2)}(0)$ which describes the intensity fluctuations of the signal emission is reduced to a value close to 1 as it happens for a coherent field.

B. Above the parametric instability threshold

1. Far-field angular pattern

As the pump frequency ω_p goes through the critical value $\omega_p^{(c)}$, the signal and idler emission concentrates in a single signal/idler pair of modes at $\mathbf{k}_{s,i}$ and their intensity becomes of the same order as the one in the pump mode at $\mathbf{k}_p$ (Fig. 5).

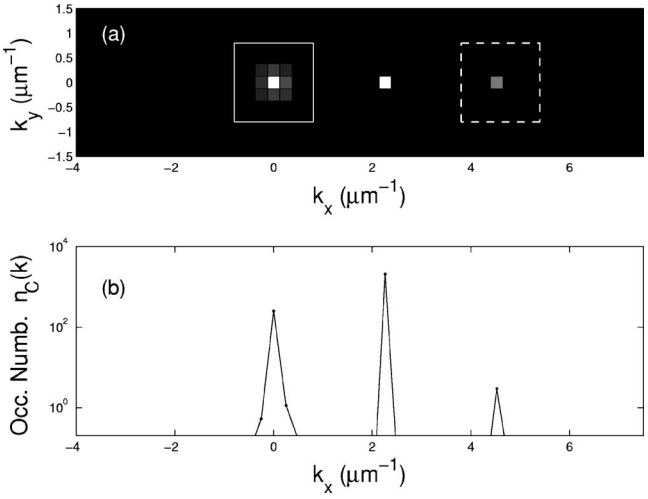

FIG. 5. (a) Far-field emission pattern for a pump frequency $\hbar\delta_p=-0.5$ meV (above the mean-field threshold). The solid (dashed) rectangles indicate the **k**-space region which forms the signal (idler) emission. Throughout the whole paper, the correlation functions of the selected signal emission are denoted with a bar (e.g., $\bar{G}^{(2)}$ and $\bar{g}^{(1,2)}$). (b) Cut for $k_y=0$ of the far-field emission pattern shown in panel (a). The cavity and the other pump parameters are the same as in Fig. 1.

In Fig. 6 we have plotted the intensity in the pump and the signal modes as a function of the pump frequency ω_p. While the pump intensity N_p is simply the occupation number $n_C(\mathbf{k}_p)$ of the mode at $\mathbf{k}_p$, the signal and idler intensities $N_{s,i}$ are defined as the sum of the occupation numbers $n_C(\mathbf{k})$ for **k** within the regions contained in, respectively, the solid and dashed rectangles in Fig. 5.

Both the pump and the signal intensities show a threshold behavior at $\omega_p^{(c)}$: the pump intensity N_p monotonically increases upto the threshold, and then starts slightly decreasing because of the presence of the finite signal [Fig. 6(a)]. The signal one N_s is very weak below the threshold, and has a sudden increase close to $\omega_p^{(c)}$ [Fig. 6(b)]. As compared to the mean-field prediction,[47] the transition is rounded by quantum fluctuations, which give indeed a finite signal intensity also below the threshold and smoothen the threshold. Note that fluctuations are also responsible for the slight shift of the threshold which can be observed in the figure. The behavior of the idler intensity (not shown) is strictly analogous to the one of the signal one.

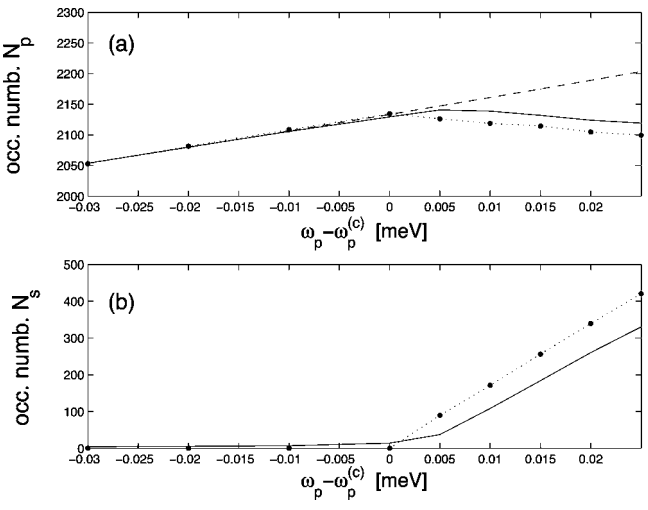

FIG. 6. Intensity in the pump (a) and signal (b) modes as a function of the pump frequency ω_p. Solid lines: Wigner–Monte Carlo results. Dotted lines: mean-field prediction. The dashed line in panel (a) gives the intensity in the pump mode for the unstable homogeneous mean-field state of Eqs. (13) and (14). The cavity and the other pump parameters are the same as in Fig. 1.

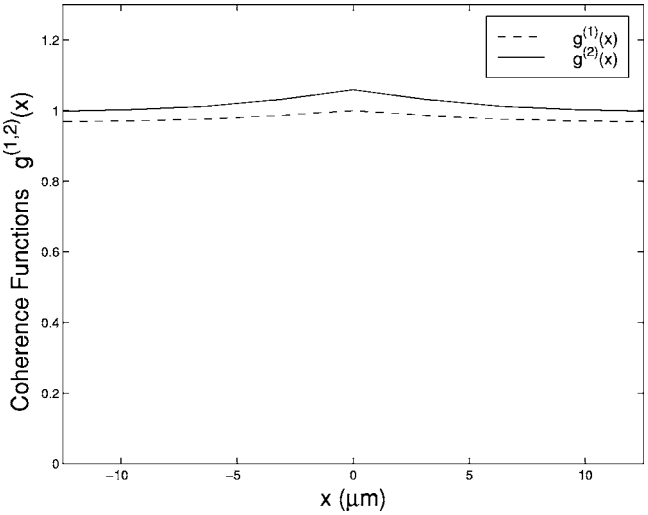

FIG. 7. First- (dashed) and second-order (solid) coherence functions $\bar{g}^{(1,2)}(\mathbf{x})$ of the selected (see solid rectangle in Fig. 2) signal emission for a pump frequency $\hbar\delta_p^{(c)}=-0.5$ meV (above the mean-field threshold). The cavity and the other pump parameters are the same as in Fig. 1.

Far above the threshold, additional, weaker, peaks appear due to multiple scattering processes,[9] but they are filtered out when the signal emission is selected. A discussion of these coherent peaks, as well as of the novel spectral and angular features shown by the weak incoherent luminescence when we are far above the threshold go beyond the scope of the present paper and will be postponed to future work.

2. First- and second-order coherence function

As in Sec. V A 2, we have selected the region *S* in wave-vector space corresponding to the signal emission (within the solid rectangle in Fig. 5) and we have determined its coherence properties. The first- and second-order coherence functions $\bar{g}^{(1,2)}(\mathbf{x})$ are plotted in Fig. 7. $\bar{g}^{(1)}(\mathbf{x})$ is nearly flat and equal to 1, which indicates that the first-order coherence extends over the whole two-dimensional sample or, in other terms, that the emission is phase coherent. As expected for a coherent field, the second-order coherence function $\bar{g}^{(2)}(\mathbf{x})$ is also almost flat and its value close to 1: in physical terms, this means that the intensity fluctuations of the signal emission are weak. Both these qualitative behaviors are in agreement with the experimental observations reported in Ref. 7.

VI. ANALOGY WITH THE BOSE GAS AT THERMAL EQUILIBRIUM

The analogy between the threshold of an optical parametric oscillator or of a laser and a sort of non-equilibrium second-order phase transition was put forward in the 1970s,[14,15] but its study was mostly focussed on the case of few-mode systems, such as optical resonators with discrete modes. Its generalization to spatially extended systems showing a continuum of modes is instead a much more recent topic from both the theoretical[27] and the experimental[7] points of view. In the present section, we shall try to interpret the results presented in the previous section in terms of a sort of nonequilibrium Bose-Einstein condensation.

At the level of mean-field theory, the analogy is immediate: in usual statistical mechanics, the onset of a phase transition is signalled by the thermodynamical instability of the symmetric state and the consequent appearance of a nonvanishing value of the order parameter in the equilibrium state. For the specific case of the Bose-Einstein condensation transition, the order parameter consists of the expectation value of the Bose field $\hat{\Psi}(\mathbf{x})$.

In the present nonequilibrium case, the mean-field threshold corresponds to the point where the homogeneous solutions (13) and (14) become unstable and a finite signal and idler amplitudes appear in the new stable stationary state. As in the standard theory of the optical parametric oscillator, the absolute phases of the signal and the idler are not fixed by the dynamics. The Hamiltonian is in fact invariant under the U(1) symmetry which sends $\psi^{(s,i)} \rightarrow \psi^{(s,i)} e^{\pm i\theta}$ and the specific value of the signal phase is randomly chosen at each realization by the spontaneous symmetry breaking mechanism. The chosen value of the order parameter is the same throughout the whole system.

Quantitative results to illustrate the physics of this spontaneous symmetry breaking are obtained from the Wigner–Monte Carlo calculations including the fluctuations around the meanfield which smoothens the threshold. Because of the fluctuations, the signal and idler amplitudes no longer vanish below threshold, but as the signal and idler emissions take place into many available modes which are close to resonance, they are incoherent both spatially and temporally. As the threshold is approached, the characteristic coherence length which determines the spatial behavior of the first- and second-order coherence functions $\bar{g}^{(1,2)}(\mathbf{x})$ increases and becomes macroscopic at the threshold. Simultaneously, the intensity fluctuations, quantified by $\bar{g}^{(2)}(0)$, are quenched.

Above the threshold, the parametric emission is concentrated in a single pair of modes, whose amplitude is accurately described by a **C** number as in the mean-field theory. Fluctuations give only a small correction. In particular, the signal and idler phases are constant throughout the whole two-dimensional sample. As it is usual in the spontaneous symmetry breaking phenomena, this does not violate the U(1) symmetry of the system Hamiltonian, since the phase is chosen at random.

These behaviors are strictly analogous to what happens in a Bose gas at thermal equilibrium when the temperature is lowered across the Bose-Einstein condensation temperature T_{BEC}. For $T > T_{\mathrm{BEC}}$, the gas is a thermal, incoherent, one and is spread among many low-lying modes. Its coherence extends for a finite distance, generally smaller than the interparticle spacing, and the same coherence length determines the spatial behavior of both the phase (first-) and the density-density (second-order) correlation function of the gas. For $T \rightarrow T_{\mathrm{BEC}}^{+}$, the coherence length diverges.[6,12] For $T < T_{\mathrm{BEC}}$ a macroscopic population is concentrated in the single state of lowest energy and an off-diagonal long-range order appears in the real-space one-body density matrix. This is the so-called Penrose-Onsager criterion for Bose-Einstein condensation.[13]

Also from the experimental point of view there is a close relation between experiments such as the ones in Ref. 7 which measure the coherence of the light emission, and experiments which address the coherence of the atomic matter waves. The first-order coherence of the matter wave of an atomic BEC has in fact been revealed by looking at the interference fringes formed by two atomic wavepackets extracted at different spatial positions,[37] while the density fluctuations [quantified by $g^{(2,3)}(0)$] have been measured from the interaction energy[38] and the three-body recombination rate:[39] both of them are quenched as T is lowered below T_{BEC}.

Although the analogy is very close, it is important to stress the fundamental differences between the Bose-Einstein condensation phenomenon of equilibrium statistical mechanics and the appearance of spontaneous coherence in the parametric emission from the present microcavity system. As polaritons have a finite lifetime, they have to be continuously injected in the system by an external pump, and the stationary state arises as a sort of dynamical equilibrium between the injection and the dissipation. Instead of a true thermodynamical equilibrium, we are therefore dealing with the stationary state of a driven-dissipative system.[40] Hence, there is no reason for the critical properties to be the same, and the general theorems of equilibrium statistical mechanics do not necessarily apply.

VII. MODULATIONAL INSTABILITY AND QUANTUM IMAGES

An alternative interpretation of the parametric instability can be put forward in terms of modulational instability, the initially spatially homogeneous intensity profile becoming unstable with respect to a periodic modulation which breaks the translational symmetry. Behaviors of this kind are well known in the framework of nonlinear dynamics and pattern formation,[40] and have analogies with the transition from the liquid to a crystalline solid state. The concept of modulational instability has recently played a central role in the understanding of experiments with atomic Bose-Einstein condensates.[41]

The physical origin of the intensity modulation and its relation with the parametric instability can be understood by looking at the intensity modulation pattern formed by the interference of the pump, the signal and the idler. In **k** space, the pump, the signal and the idler are localized around, respectively, $\mathbf{k}_p$, $\mathbf{k}_s$, and $\mathbf{k}_i = 2\mathbf{k}_p - \mathbf{k}_s$ and the polariton wave function can be written as

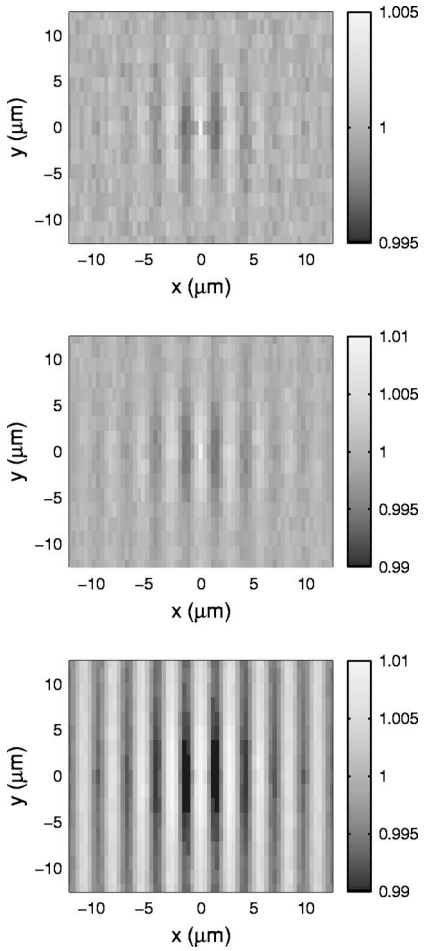

FIG. 8. Intensity correlation function $G^{(2)}(\mathbf{x})$ of the in-cavity polariton field for values of the pump frequency $\hbar\delta_p=-0.55$ meV (upper panel), $\hbar\delta_p=-0.53$ meV (central panel), and $\hbar\delta_p=-0.52$ meV (lower panel), respectively, below and around the mean-field threshold. The cavity and the other pump parameters are the same as in Fig. 1.

$$\psi_i(\mathbf{x}) = \psi_i^{(p)} e^{i\mathbf{k}_p\cdot\mathbf{x}} + \psi_i^{(s)}(\mathbf{x}) e^{i\mathbf{k}_s\cdot\mathbf{x}} + \psi_i^{(i)}(\mathbf{x}) e^{i\mathbf{k}_i\cdot\mathbf{x}}, \qquad (32)$$

where $\psi_i^{(s,i)}(\mathbf{x})$ are slowly varying functions as compared to the period $\ell_\rho = 2\pi/|\mathbf{k}_p - \mathbf{k}_s|$ of the intensity modulation. As a shift of the signal and idler phases by $\pm\phi$ corresponds to a spatial translation of the intensity modulation pattern by $\Delta x = \ell_\rho \phi/2\pi$ along the direction of $\mathbf{k}_s - \mathbf{k}_p$, the spontaneous breaking of the U(1) symmetry corresponding to the signal and idler phases can also be interpreted as the spontaneous breaking of the translational symmetry along the direction of $\mathbf{k}_p - \mathbf{k}_s$. As the position of the fringes is random, the mean intensity profile remains flat, which guarantees that the translational invariance of the system Hamiltonian (1) is preserved.

On the other hand, fringes appear clearly in the intensity correlation function of the polariton field

$$G^{(2)}(\mathbf{x}) = \langle \hat{\Psi}_C^\dagger(\mathbf{y}) \hat{\Psi}_C^\dagger(\mathbf{y}+\mathbf{x}) \hat{\Psi}_C(\mathbf{y}+\mathbf{x}) \hat{\Psi}_C(\mathbf{y}) \rangle, \qquad (33)$$

which is plotted in Fig. 8. Experimentally, $G^{(2)}(\mathbf{x})$ can be measured by simply isolating in the near-field the light emitted from a pair of points $\mathbf{y}$ and $\mathbf{y}+\mathbf{x}$ spaced of $\mathbf{x}$ and then correlating the corresponding intensity fluctuations. As the intensity pattern arises from the interference of signal, pump and idler modes, no preliminary angular selection must now be performed and, for this reason, the symbol $G^{(2)}(\mathbf{x})$ does not carry a bar over it.

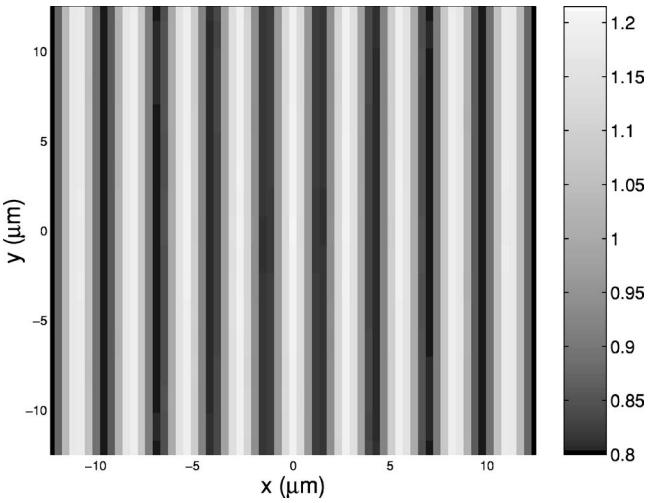

FIG. 9. Intensity correlation function $G^{(2)}(\mathbf{x})$ of the in-cavity polariton field for a pump frequency $\hbar\delta_p=-0.5$ meV above the threshold. The cavity and the other pump parameters are the same as in Fig. 1.

A detailed study of the appearance of the fringes, effect which in quantum optics goes under the name of "quantum images,"[42] was given in Ref. 27 for the simple case of an optical parametric oscillator formed by a $\chi^{(2)}$ medium in a planar cavity. Here we want to emphasize the relation between the phase coherence properties of the signal/idler emission, quantified by $\bar{g}^{(1)}(\mathbf{x})$ defined in Eq. (28) and the coherence length of the periodic modulation of $G^{(2)}(\mathbf{x})$. As a shift of the signal and idler phases by $\pm\phi$ corresponds to a spatial translation displacement of the intensity pattern, a spatial rigidity of the phase of $\psi^{(s,i)}(\mathbf{x})$ transfers into a corresponding rigidity of the intensity modulation pattern. On the other hand, when the phase of $\psi^{(s,i)}(\mathbf{x})$ is able to freely fluctuate in space, the intensity modulation pattern is washed out. This can be observed in Figs. 8 and 9 which show $G^{(2)}(\mathbf{x})$ for the two cases respectively below and above the threshold: in the first case, the spatial extension of the modulation pattern is finite and equal to the phase coherence length ℓ_c, while in the second case the pattern extends over the whole system. A related interference effect has been used in Ref. 26 to infer the coherence length of an atomic Bose-Einstein condensate from a measurement of intensity correlations.

In Ref. 28, the spontaneous breaking of translational symmetry in a planar optical parametric oscillator was pointed out as a slowing down of the diffusive motion of the modulation pattern during the time evolution of a single realization. Here we show another interesting consequence of the same phenomenon in the intensity profile of a single realization of the Wigner–Monte Carlo, that is in an instantanous measurement of the local intensity. While below threshold

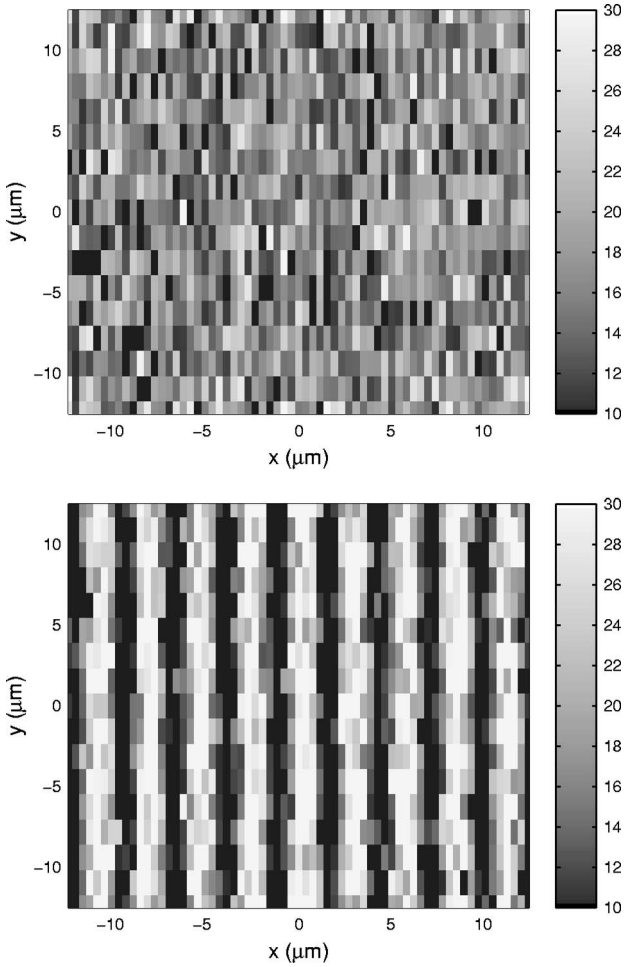

FIG. 10. Intensity profile $\psi_C(\mathbf{x})|^2|$ of a single realization for pump frequencies $\hbar\delta_p=-0.53$ meV (upper panel) and $\hbar\delta_p=-0.5$ meV (lower panel), respectively, below and above the mean-field threshold. The cavity and the other pump parameters are the same as in Fig. 1, exception made for the coupling constant g and the driving intensity I_p, respectively, increased and decreased by a factor 5 so as to clarify the picture without affecting the mean-field physics.

the modulation pattern is too weak to be detected on a single realization and has to be obtained by taking the average over many realizations, it appears clearly although somewhat noisy in a picture taken above threshold when the occupation of the signal and idler modes is large and coherent (Fig. 10). Obviously, the position of the pattern is random and varies from one realization to the next.

VIII. ONE-DIMENSIONAL SYSTEM: LOCAL VS GLOBAL COHERENCE

All the physical discussions presented in the previous sections were based on a mean-field picture: below threshold, many modes are incoherently populated, while above threshold, there is a macroscopic occupation of a single signal/idler pair of mode and fluctuations give only a small correction. This interpretation was validated by the numerical results of the complete Wigner–Monte Carlo simulations which were

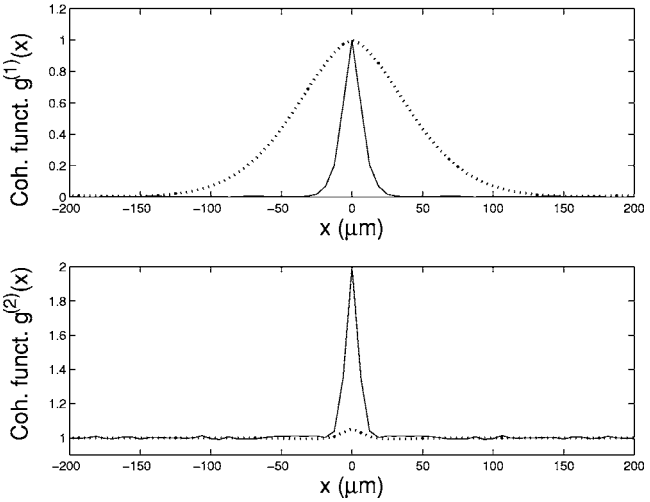

FIG. 11. First- (upper panel) and second-order (lower panel) coherence functions $\bar{g}^{(1,2)}(\mathbf{x})$ of the selected signal emission for pump frequencies, respectively, $\hbar\delta_p=-0.53$ meV below the mean-field threshold (solid) and $\hbar\delta_p=-0.51$ meV above the mean-field threshold (dotted). The cavity and the other pump parameters are the same as in Fig. 1, exception made for the geometry: the system is here one-dimensional and $L_x=400$ μm.

performed for two-dimensional systems of side $L_x=L_y=25$ μm: above the threshold, coherence of the signal emission extended over the whole two-dimensional sample giving a sort of nonequilibrium long-range order.

It is a well-known fact of equilibrium statistical mechanics that the spontaneous breaking of a U(1) symmetry and the appearance of a long-range order is possible only in dimension $d>2$ at finite temperature and in $d\geqslant 2$ at zero temperature (Mermin-Wagner theorem[43,44]), while otherwise coherence extends over a finite distance only. In order to investigate the possibility of observing such behaviors in a nonequilibrium context, we have performed Wigner–Monte Carlo simulations for a system with the same pump parameters as in the previous sections, but in a completely different cavity geometry. Instead of a square of size $L_x=L_y=25$ μm, we consider here a one-dimensional system of length $L_x=400$ μm. Along this axial direction, the polaritons are free and periodic boundary conditions are assumed, while the transverse motion is assumed to be frozen in the lowest state by a strong lateral confinement. This kind of reduced-dimensionality systems are well within the possibilities of actual semiconductor technology: effectively one-dimensional systems has been recently demonstrated by several groups.[23]

The results of numerical calculations for the first- and second-order coherence of the signal emission are shown in Fig. 11: below the threshold, the behavior is similar to the one already observed in the two-dimensional case (Figs. 3 and 4): the phase coherence extends over a finite distance and intensity fluctuations due to the Hanbury-Brown and Twiss bunching effect are important $\bar{g}^{(2)}\approx 2$. Above the threshold, the intensity fluctuations are strongly suppressed $\bar{g}^{(2)}\approx 1$ as in the two-dimensional case of Fig. 7, while the phase coherence of the signal extends over a longer but still finite distance. The large distance limit of $\bar{g}^{(1)}$ is in fact 0 and

no long-range coherence exists. Similar results were discussed in Ref. 28 for the case of a roll-pattern instability in an optical cavity.

In the language of equilibrium statistical mechanics, phenomena of this kind are well-known and usually go under the name of "quasi condensates,"[24–26] so to stress the fact that a local order is present (signalled by the reduced value of the intensity fluctuations), but not the global one which characterizes a true Bose-Einstein condensate. The long-range order is in fact destroyed by the long wavelength fluctuations of the order parameter, in our case the local phase of the signal emission.[48]

A final remark: recently, the realization of a BEC of polaritons was claimed in Ref. 10 starting from the observation of a reduced value of $\bar{g}^{(2)}$. Unless a detailed analysis of the geometry of the system is performed, this observation does not appear as being a conclusive proof of polariton BEC, as the mere reduction of intensity fluctuations does not univocally correspond to the presence of a long-range order. In other terms, the possibility of having a quasicondensate of polaritons has not been ruled out by the available experimental data.

IX. CONCLUSIONS AND PERSPECTIVES

In the present paper we have presented a comprehensive study of the coherence properties of the parametric emission from a planar semiconductor microcavity for pump parameters spanning across the threshold for the parametric oscillation. The numerical calculations have been performed by means of a Monte Carlo technique based on the stochastic differential equations of the Wigner representation of the coupled exciton and cavity-photon quantum fields. Inspired by the first experimental results reported in Ref. 7, we have calculated the coherence properties of the in-cavity polaritonic field and, more specifically, of the light which is then emitted in the signal beam. In particular, we have analyzed the behavior of the first and the second-order coherence functions when the pump parameters cross the threshold for the parametric oscillation. The numerical results are physically understood in terms of a nonequilibrium phase transition occurring at the parametric threshold, a phase transition which closely ressembles to a nonequilibrium Bose-Einstein condensation.

Below threshold, the emission is an incoherent one, and the first- and second-order correlation functions show a finite coherence length for both the phase correlation and the intensity fluctuations. As the pump approaches the threshold, the coherence length becomes larger and larger and eventually becomes macroscopic at the threshold. In momentum space, this corresponds to a broad momentum distribution which gets narrowed into a deltalike peak at the threshold. Above threshold, the emission is instead a coherent one, both the signal and the idler intensities becoming of the same order as the pump one, and the corresponding momentum distribution being sharply peaked. For two-dimensional systems of size comparable to the one of actual experiments with planar microcavities, first- and second-order coherence extends in the whole system. For systems of reduced dimensionality such as photon wires, the numerical results suggest that a local order persists in the sense that intensity fluctuations are strongly reduced, but no true long-range order is present, as the global phase coherence is destroyed by long-wavelength phase fluctuations. This phenomenon is a nonequilibrium analog of the so-called quasicondensation phenomenon of reduced-dimensionality Bose gases at equilibrium.

Although the results of the present paper have been obtained for a very specific system of actual experimental interest, we expect the main properties of the critical point at the threshold to be very general for a whole class of nonequilibrium systems. Also the absence of long-range order in low-dimensional systems is expected to be a general fact in nonequilibrium systems: inspired by the Mermin-Wagner theorem of equilibrium statistical mechanics, we are actually trying to characterize the possibility of a long-range order in non-equilibrium systems of reduced dimensionality, and to determine the corresponding phase coherence length. In order to have a closer comparison with experiments, the effect of a disorder [which can be straightforwardly taken into account via the potentials $V_{X,C}(\mathbf{x})$ in Eq. (1)] on the nonequilibrium critical properties will be adressed as well.

ACKNOWLEDGMENTS

Continuous stimulating discussions with A. Baas, O. El Daïf, J. Tignon, G. Dasbach, C. Diederichs, A. Verger, Y. Castin, C. Lobo, A. Sinatra, C. Tozzo, F. Dalfovo, V. Savona, and A. Rosso are warmly acknowledged. I.C. is grateful to M. Wouters for his active interest on polaritonic quasicondensation issues.

*Electronic address: carusott@science.unitn.it

[1] *Confined Electrons and Photons*, edited by E. Burstein and C. Weisbuch (Plenum Press, New York, 1995).

[2] *Proceedings of the International School of Physics "Enrico Fermi," Course CL: Electron and Photon Confinement in Semiconductor Nanostructures*, edited by B. Deveaud, A. Quattropani, and P. Schwendimann (IOS Press, Amsterdam, 2003).

[3] Special issue on Microcavities, edited by J. Baumberg and L. Viña [Semicond. Sci. Technol. **18**, S279 (2003)].

[4] I. Carusotto and C. Ciuti, Phys. Rev. Lett. **93**, 166401 (2004); C. Ciuti and I. Carusotto, Phys. Status Solidi B **242**, 2224 (2005).

[5] D. Pines and P. Nozieres, *The Theory of Quantum Liquids* (Addison-Wesley, Redwood City, 1966), Vols. 1 and 2.

[6] L. Pitaevskii and S. Stringari, *Bose-Einstein Condensation* (Oxford University Press, Oxford, 2003).

[7] A. Baas, J.-Ph. Karr, M. Romanelli, A. Bramati, and E. Giacobino, cond-mat/0501260 (unpublished).

[8] P. G. Savvidis, J. J. Baumberg, R. M. Stevenson, M. S. Skolnick, D. M. Whittaker, and J. S. Roberts, Phys. Rev. Lett. **84**, 1547 (2000); R. M. Stevenson, V. N. Astratov, M. S. Skolnick, D. M.

Whittaker, M. Emam-Ismail, A. I. Tartakovskii, P. G. Savvidis, J. J. Baumberg, and J. S. Roberts, *ibid.* **85**, 3680 (2000); R. Houdré, C. Weisbuch, R. P. Stanley, U. Oesterle, and M. Ilegems, *ibid.* **85**, 2793 (2000); A. Huynh, J. Tignon, O. Larsson, Ph. Roussignol, C. Delalande, R. André, R. Romestain, and Le Si Dang, *ibid.* **90**, 106401 (2003).

[9] P. G. Savvidis, C. Ciuti, J. J. Baumberg, D. M. Whittaker, M. S. Skolnick, and J. S. Roberts, Phys. Rev. B **64**, 075311 (2001).

[10] H. Deng, G. Weihs, C. Santori, J. Bloch, and Y. Yamamoto, Science **298**, 199 (2002).

[11] For a review about exciton BEC, see *Bose-Einstein Condensation*, edited by A. Griffin, D. W. Snoke, and S. Stringari (Cambridge University Press, Cambridge, 1995). Recent experiments in this direction are reported, e.g., by L. V. Butov, C. W. Lai, A. L. Ivanov, A. C. Gossard, and D. S. Chemla, Nature (London) **417**, 47 (2002); D. Snoke, S. Denev, Y. Liu, L. Pfeiffer, and K. West, *ibid.* **418**, 754 (2002); J. P. Eisenstein and A. H. MacDonald, *ibid.* **432**, 691 (2004), and references therein.

[12] C. Cohen-Tannoudji, lecture notes at the Collége de France, 1999–2000.

[13] O. Penrose and L. Onsager, Phys. Rev. **104**, 576 (1956).

[14] V. Degiorgio and M. O. Scully, Phys. Rev. A **2**, 1170 (1970); R. Graham and H. Haken, Z. Phys. **237**, 31 (1970).

[15] M. O. Scully and M. S. Zubairy, *Quantum Optics* (Cambridge University Press, Cambridge, 1997).

[16] D. F. Walls and G. J. Milburn, *Quantum Optics* (Springer, Berlin, 1994).

[17] For a review, see C. Ciuti, P. Schwendimann, and A. Quattropani, Semicond. Sci. Technol. **18**, S279 (2003), and references therein.

[18] C. Ciuti, P. Schwendimann, and A. Quattropani, Phys. Rev. B **63**, 041303(R) (2001).

[19] V. Savona, P. Schwendimann, and A. Quattropani, Phys. Rev. B **71**, 125315 (2005).

[20] C. Ciuti, P. Schwendimann, B. Deveaud, and A. Quattropani, Phys. Rev. B **62**, R4825 (2000).

[21] D. M. Whittaker, Phys. Rev. B **63**, 193305 (2001).

[22] D. M. Whittaker, Phys. Rev. B **71**, 115301 (2005).

[23] G. Dasbach, M. Schwab, M. Bayer, and A. Forchel, Phys. Rev. B **64**, 201309(R) (2001); G. Dasbach, M. Schwab, M. Bayer, D. N. Krizhanovskii, and A. Forchel, *ibid.* **66**, 201201(R) (2002); G. Dasbach, C. Diederichs, J. Tignon, C. Ciuti, Ph. Roussignol, C. Delalande, M. Bayer, and A. Forchel, Phys. Rev. B **71**, 161308 (2005).

[24] Y. Castin, lecture notes at the Les Houches school on Low dimensional quantum gases [J. Phys. IV (France), **116**, 89 (2004)], and references therein.

[25] S. Dettmer, D. Hellweg, P. Ryytty, J. J. Arlt, W. Ertmer, K. Sengstock, D. S. Petrov, G. V. Shlyapnikov, H. Kreutzmann, L. Santos, and M. Lewenstein, Phys. Rev. Lett. **87**, 160406 (2001); S. Richard, F. Gerbier, J. H. Thywissen, M. Hugbart, P. Bouyer, and A. Aspect, *ibid.* **91**, 010405 (2003).

[26] D. Hellweg, L. Cacciapuoti, M. Kottke, T. Schulte, K. Sengstock, W. Ertmer, and J. J. Arlt, Phys. Rev. Lett. **91**, 010406 (2003).

[27] A. Gatti and L. Lugiato, Phys. Rev. A **52**, 1675 (1995).

[28] R. Zambrini, M. Hoyuelos, A. Gatti, P. Colet, L. Lugiato, and M. San Miguel, Phys. Rev. A **62**, 063801 (2000).

[29] P. G. Lagoudakis, P. G. Savvidis, J. J. Baumberg, D. M. Whittaker, P. R. Eastham, M. S. Skolnick, and J. S. Roberts, Phys. Rev. B **65**, 161310(R) (2002); I. Shelykh, G. Malpuech, K. V. Kavokin, A. V. Kavokin, and P. Bigenwald, *ibid.* **70**, 115301 (2004).

[30] Diffusion Monte Carlo calculations have been performed only for three-dimensional excitons in bulk materials, see J. Shumway and D. M. Ceperley, Phys. Rev. B **63**, 165209 (2001).

[31] C. Ciuti, V. Savona, C. Piermarocchi, A. Quattropani, and P. Schwendimann, Phys. Rev. B **58**, 7926 (1998); F. Tassone and Y. Yamamoto, *ibid.* **59**, 10 830 (1999).

[32] See, e.g., J. E. Curtis and D. G. Grier, Phys. Rev. Lett. **90**, 133901 (2003).

[33] M. J. Steel, M. K. Olsen, L. I. Plimak, P. D. Drummond, S. M. Tan, M. J. Collett, D. F. Walls, and R. Graham, Phys. Rev. A **58**, 4824 (1998); A. Sinatra, C. Lobo, and Y. Castin, J. Phys. B **35**, 3599 (2002).

[34] P. Schwendimann, C. Ciuti, and A. Quattropani, Phys. Rev. B **68**, 165324 (2003).

[35] J. Ph. Karr, A. Baas, R. Houdré, and E. Giacobino, Phys. Rev. A **69**, 031802(R) (2004); J. Ph. Karr, A. Baas, and E. Giacobino, *ibid.* **69** 063807 (2004).

[36] R. Hanbury-Brown and R. W. Twiss, Nature (London) **177**, 27 (1956).

[37] I. Bloch, T. W. Hänsch, and T. Esslinger, Nature (London) **403**, 166 (2000).

[38] W. Ketterle and H.-J. Miesner, Phys. Rev. A **56**, 3291 (1997).

[39] E. A. Burt, R. W. Ghrist, C. J. Myatt, M. J. Holland, E. A. Cornell, and C. E. Wieman, Phys. Rev. Lett. **79**, 337 (1997).

[40] M. C. Cross and P. C. Hohenberg, Rev. Mod. Phys. **65**, 851 (1993).

[41] L. Fallani, L. De Sarlo, J. E. Lye, M. Modugno, R. Saers, C. Fort, and M. Inguscio, Phys. Rev. Lett. **93**, 140406 (2004).

[42] L. Lugiato and G. Grynberg, Europhys. Lett. **29**, 675 (1995).

[43] K. Huang, *Statistical Mechanics* (Wiley, New York, 1997).

[44] P. C. Hohenberg, Phys. Rev. **158**, 383 (1967); N. D. Mermin and H. Wagner, Phys. Rev. Lett. **17**, 1133 (1966).

[45] If a theoretical prediction for the lattice coupling constant g is needed, the same procedure as used in the case of ultracold atoms could be adopted [see, e.g., C. Mora and Y. Castin, Phys. Rev. A **67**, 053615 (2003).]: the value of g is chosen in such a way that the scattering T matrix on the lattice best approximates the physical scattering T matrix of the continuum problem. Unless the T matrix shows narrow Feshbach resonances in the region of interest, this procedure provides a very good approximation of the low-energy scattering properties.

[46] The analysis of the reflected light requires more attention: the field emitted by the cavity through the front mirror has in fact to be added to the direct reflection of the pump beam on the front mirror.

[47] This can be numerically obtained by means of the same Wigner–Monte Carlo code by taking the mean-field limit (Ref.) $g \to 0, E_p \to \infty$ at a fixed $g|E_p|^2$ (i.e., at a fixed interaction energy $g|\psi_X|^2$). See, e.g., Y. Castin, in *Coherent Atomic Matter Wves*, Lecture Notes of Les Houches Summer School, edited by R. Kaiser, C. Westbrook, and F. David (Springer-Verlag, Berlin, 2001), pp. 1–136.

[48] In principle, a similar quasi condensation behavior may show up in two-dimensional systems as well, but the distinction between a condensate and a quasi-condensate may require very large samples to rule out the possibility of a finite-size-induced BEC (Ref. 6). Analytical work in this direction is under way.